Photon-number statistics from resonance fluorescence of a two-level atom near a plasmonic nanoparticle

Vladimir M. Pastukhov,* Yulia V. Vladimirova, and Victor N. Zadkov,†
International Laser Center and Faculty of Physics, M. V. Lomonosov Moscow State University, Moscow 119992, Russia
(Received 16 July 2014; published 22 December 2014)

The photon-number statistics from resonance fluorescence of a two-level atom near a metal nanosphere driven by a laser field with finite bandwidth is studied theoretically. Our analysis shows that all interesting physics here takes place in a small area around the nanosphere where the near field and the atom-nanosphere coupling essentially affect the radiative properties of the atom. Computer modeling estimates this area roughly as $r \leqslant 2a$ (r is the distance from the center of the nanosphere to the atom), with a being the radius of the nanosphere. At the larger distances, the influence of the nanoparticle vanishes and the atom tends to behave similarly to that in free space. It is shown that the distribution function $p(n,T)$ of the emission probability of n photons in a given time interval T in steady-state resonance fluorescence drastically depends on the atom location around the nanosphere for $r \leqslant 2a$, featuring a characteristic twist in the ridgelike dependence and a convergence time of up to 9 μs, two orders of magnitude slower than for the atom in free space. At large distances, the distribution converges to a Gaussian one, as for the atom in free space. The typical convergence time scale at large distances $r > 2a$ tends to the convergence time of the atom in free space. There are also two areas symmetrical around the nanosphere in which $\Omega \sim \gamma$ and the convergence time goes to zero. This behavior is determined by the interplay of the radiative and nonradiative decay rates of the atom due to the coupling with the metal nanosphere and by the near-field intensity. Additional parameters are the normalized laser frequency detuning from the atomic resonance and the bandwidth of the incoming laser field.

DOI: 10.1103/PhysRevA.90.063831 PACS number(s): 42.50.Ar, 33.50.−j, 68.37.Uv, 73.20.Mf

I. INTRODUCTION

The nonclassical behavior of light has been revealed at the single-atom level in resonance fluorescence as the sub-Poissonian behavior of the photon-number statistics and the phenomenon of antibunching of scattered photons [1–3]. The first experimental confirmation of the antibunching of photons in resonance fluorescence was made by Kimble *et al.* [4] and the sub-Poissonian photon-number statistics was later verified by Short and Mandel [5]. Observation of the nonclassical properties of resonance fluorescence from a single trapped atomic ion was made by Diedrich and Walther [6].

Over the two past decades, such a single-atom level of experiments for studying nonclassical light from isolated atoms or ions was also achieved in the emerging field of nanophotonics [7], which demonstrates reliable sources of nonclassical light from single molecules [8,9], quantum dots [10–14], and nitrogen-vacancy centers in nanodiamonds [15,16], including those embedded in different nanostructures. In this case, the radiative properties of an emitter (atom, molecule, or quantum dot) are strongly modified in confined geometries [17–19]. Plasmonic nanostructures, specifically metal nanoparticles [20–22], not only convert the incoming radiation to localized [23], but also change the radiative frequency of the emitter and its decay rate [19]. This leads to one of the important applications of nano-optics: using plasmonic nanostructures for changing and controlling fluorescence.

The resonance fluorescence, which features the nonclassical behavior of fluorescent light, occurs when the quantum emitter is driven by an electromagnetic field with the frequency close to the emitter's resonant frequency [24] and studying the resonance fluorescence of a quantum emitter near a metal nanoparticle is just at the initial stages [25–28]. These few theoretical papers target the spectrum of resonance fluorescence and not much attention has been paid so far to the nonclassical behavior of scattered light.

In this paper we study the photon-number statistics in resonance fluorescence of a two-level atom near a metal nanoparticle, which we consider for simplicity a metal nanosphere, driven by a laser field with finite bandwidth, as a function of the atom's location around the nanoparticle, the intensity of the incident laser field, its bandwidth, and the detuning from the atomic resonance. We have restricted ourselves to the case of a two-level atom because we want to study the principal features of the nonclassical light from resonance fluorescence near a metal nanoparticle. However, our approach can also be generalized to multilevel atoms in a manner analogous to the method applied for multilevel atoms in free space [29–31].

The arrangement of the problem is given in Fig. 1. A two-level atom with a dipole moment $\mathbf{d}$ is placed in close proximity to the metal nanosphere of radius $a = 20$ nm located at the origin of the coordinate system. The atom's location is defined by its radial coordinate $|\mathbf{r}|$ and the polar angle θ (in the spherical coordinate system); ε and ε_1 are the permittivities of the metal the nanosphere is made of and the space our atom-nanosphere system is placed in, respectively. For further calculations we assume that the nanosphere is made of silver: Its permittivity is equal to $\varepsilon = -15.37 + i0.231$ and the wavelength of the incident laser field $\lambda = 632.8$ nm. We also assume for simplicity that $\varepsilon_1 = 1$. The incoming z-polarized laser radiation $\mathbf{E}_0$ with the frequency ω_L, which is close to

*Present address: Mathematical Sciences, Lund University, SE221 00 Sweden.
†zadkov@phys.msu.ru

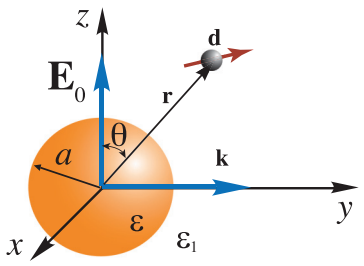

FIG. 1. (Color online) Arrangement of the metal nanosphere plus atom system driving by the incident laser field $\mathbf{E}_0$. The resonance fluorescence is detected by a 4π photodetector in the far field. The sizes of the metal nanoparticle and the atom are shown not to scale.

the frequency ω_0 of the atomic dipole transition, has the wave vector $\mathbf{k}$ directed along the y axis. We will also assume that the incident laser radiation has a Lorentzian spectral profile with the finite bandwidth $\Delta\omega_L = 1$ MHz and the electric field equal to $E = 1000$ V/m.

It is also important to note that the direction of the atomic dipole moment coincides with the direction of the near field created around the metal nanoparticle at the point of space the atom is located. This would not be correct for the case of a molecule or a quantum dot, however the generalization of our results to other types of a quantum emitter (molecule, molecular cluster, and quantum dot), which are not pointlike and whose direction of the dipole moment does not coincide with that of the near-field polarization at the point of space the emitter is located, is straightforward.

The paper is organized as follows. In Sec. II we give an overview of the mechanisms of modification of the near field and radiative and nonradiative decay rates of the two-level atom located in close proximity to a metal nanosphere. Simple analytical expressions are given for the near-field enhancement, the modified total decay rate of the atom near the metal nanosphere, and the frequency shift of the atomic transition. Section III A is targeted at the analysis of the photon-number statistics of light from resonance fluorescence in our system. It is shown that the distribution function $p(n,T)$ of the emission probability of n photons in a given time interval T strongly depends on the near-field intensity at the point of space the atom is located and can be controlled by a few key parameters: the atom's location around the metal nanosphere, the intensity of the incident laser field, its bandwidth, and detuning from the atomic resonance. Analytical expressions for the mean and the variance of the number of photons are derived for the case when T is much longer than the atomic transition lifetime. It is also shown that by analogy with the atom in free space [3], this distribution function converges in the distribution to a Gaussian one when T is longer than the natural lifetime of the excited atom modified by the nanoparticle. A detailed computer analysis of the convergence time, the distribution function, the mean value, and the variance is given in Sec. III B. It is shown that the typical convergence time scale is up to two orders of magnitude longer than for the case of an atom in free space. In Sec. IV we summarize the results obtained and discuss some possible applications.

II. THE ATOM'S RADIATIVE AND NONRADIATIVE DECAY RATES AND TRANSITION FREQUENCY SHIFT NEAR THE METAL NANOSPHERE

In this section we briefly discuss the modification of the near field of a metal nanoparticle and the decay rate and the radiative frequency shift of a two-level atom, which is located in close proximity to the nanoparticle, driven by a near resonance to the atomic transition laser field. For all these values, which depend on the spherical coordinates of the atom near the nanosphere, frequency, intensity, and polarization of the incident laser field and the parameters of the nanosphere and the atom, we give simple analytical formulas.

The electric-field intensity in close proximity to the nanosphere, whose size is significantly less than the wavelength $\lambda = 632.8$ nm of the incoming field, can be calculated in the quasistatic approximation, which implies that no retardation effects are taken into account. For the nanosphere of radius $a = 20$ nm in the homogeneous incident electric field, only dipole modes with $n = 1$ are excited [32] and the field outside the nanosphere is equal to

$$\begin{aligned}\mathbf{E} &= E_r\hat{\mathbf{n}}_r + E_\theta\hat{\mathbf{n}}_\theta \\ &= E_0(\cos\theta\hat{\mathbf{n}}_r - \sin\theta\hat{\mathbf{n}}_\theta) \\ &\quad + E_0\frac{a^3}{r^3}\frac{\varepsilon(\omega)-1}{\varepsilon(\omega)+2}(2\cos\theta\hat{\mathbf{n}}_r + \sin\theta\hat{\mathbf{n}}_\theta),\end{aligned} \tag{1}$$

where E_0 is the amplitude of the incident filed, $\hat{\mathbf{n}}_r$ and $\hat{\mathbf{n}}_\theta$ are the unit vectors in the spherical coordinate system, and $\varepsilon(\omega)$ is the permittivity of the metal nanosphere at the frequency ω. It is also worth noting here that in the case of a sphere $E_\varphi = 0$.

From this expression it follows that the near field has elliptical polarization as $\varepsilon(\omega)$ is a complex number. We can neglect this in the case of a linearly polarized plane electromagnetic incident field, when the phase difference between the principal components of the ellipsoid of polarization of the near field is almost equal to zero. However, it is worth noting that for the case of an elliptically polarized incident field the near field is elliptical too. Moreover, the metal nanosphere strongly modifies the degree of polarization of the incident field [33].

From Eq. (1) it also follows that the direction of the near field and its intensity strongly depend on $\mathbf{r}$, so the Rabi frequency Ω also depends on $\mathbf{r}$ and can be written as

$$\Omega(\mathbf{r}) = \frac{d}{\hbar}\sqrt{|E_r|^2 + |E_\theta|^2 + |E_\varphi|^2},$$

where the absolute values of the field components are equal to

$$\begin{aligned}|E_r| &= \left|E_0\cos\theta\left(\frac{2a^3}{r^3}\frac{\varepsilon(\omega)-1}{\varepsilon(\omega)+2}+1\right)\right|, \\ |E_\theta| &= \left|E_0\sin\theta\left(\frac{a^3}{r^3}\frac{\varepsilon(\omega)-1}{\varepsilon(\omega)+2}-1\right)\right|, \\ |E_\varphi| &= 0\end{aligned}$$

and the atomic dipole transition moment is equal to

$$d = \left(\frac{1}{4\pi\varepsilon_0}\frac{3\gamma_0\hbar c^3}{4\omega_{\text{vac}}^3}\right)^{1/2},$$

where $\omega_{\rm vac}$ is the frequency of the atomic dipole transition and γ_0 is the radiative decay rate of the atom in free space [24]. We will assume in all our further calculations that $\gamma_0 = 20$ MHz.

In a quasistatic, quasiclassical approximation, the total normalized decay rate of the atom located at the point in space with radius vector $\mathbf{r}$ and with the atomic dipole moment directed along the direction of the near field at this point can be defined as (see Sec. 6.3 of Ref. [19])

$$\frac{\gamma}{\gamma_0} = \frac{|E_r|^2(\gamma/\gamma_0)_{\rm rad} + |E_\theta|^2(\gamma/\gamma_0)_{\rm tan}}{|E_r|^2 + |E_\theta|^2}, \tag{2}$$

where $(\gamma/\gamma_0)_{\rm rad}$ and $(\gamma/\gamma_0)_{\rm tan}$ are the total normalized decay rates for the radial and tangential orientations of the atomic dipole, respectively,

$$\left(\frac{\gamma}{\gamma_0}\right)_{\rm rad} \xrightarrow{|\mathbf{k}|a\to 0} \frac{3}{2(|\mathbf{k}||\mathbf{r}|)^3}{\rm Im}\sum_{n=1}^{\infty}(n+1)^2\left(\frac{a}{|\mathbf{r}|}\right)^{2n+1}\frac{\alpha_n}{a^{2n+1}} + {\rm Re}\left(1+\frac{2\alpha_1}{|\mathbf{r}|^3}\right)^2 + O\left(\frac{1}{|\mathbf{k}|a}\right), \tag{3}$$

$$\left(\frac{\gamma}{\gamma_0}\right)_{\rm tan} \xrightarrow{|\mathbf{k}|a\to 0} \frac{3}{4(|\mathbf{k}||\mathbf{r}|)^3}{\rm Im}\sum_{n=1}^{\infty}n(n+1)\left(\frac{a}{|\mathbf{r}|}\right)^{2n+1}\frac{\alpha_n}{a^{2n+1}} + {\rm Re}\left(1-\frac{\alpha_1}{|\mathbf{r}|^3}\right)^2 + O\left(\frac{1}{|\mathbf{k}|a}\right), \tag{4}$$

where α_n are the multipole polarizabilities of the metal sphere of nth order

$$\alpha_n = a^{2n+1}\frac{\varepsilon(\omega)-\varepsilon_1}{\varepsilon(\omega)+\varepsilon_1(n+1)/n}.$$

From Eqs. (3) and (4) it follows that $(\gamma/\gamma_0)_{\rm tan}$ goes to zero when the atom approaches the surface of the nanosphere. This is due to the fact that the dipole moment induced in the metal nanosphere is almost equal in amplitude to the atomic dipole moment, but oppositely directed. As a result, an atom with dipole moment orientation tangential to the nanosphere surface has a slow decay rate, whereas an atom with a normal orientation of the atomic dipole moment to the nanosphere surface has a rather high decay rate.

The first terms in Eqs. (3) and (4) describe the nonradiative atomic decay rate, i.e., that part of the atom's energy that is converted to heat. The radiative decay rate of the atom is defined actually by the second terms in Eqs. (3) and (4). Figure 2 shows how the radiative, nonradiative, and total decay rates correspond to each other for the silver nanosphere we use in our calculations.

Figure 3(a) illustrates how the normalized Rabi frequency of the atomic transition depends on the spherical coordinates of the atom in the vicinity of a silver nanosphere. One can clearly see that the normalized Rabi frequency follows the distribution of the near field around the nanosphere revealing the local maximum at $\theta = \pi/2$ and increases with an increase of r, reaching the value of about $\Omega/\gamma \approx 6$ at large $r \gg a$ distances.

In the vicinity of a metal nanoparticle, the frequency of the dipole transition is shifted (the so-called radiative frequency shift [34]) and for a two-level atom is equal to

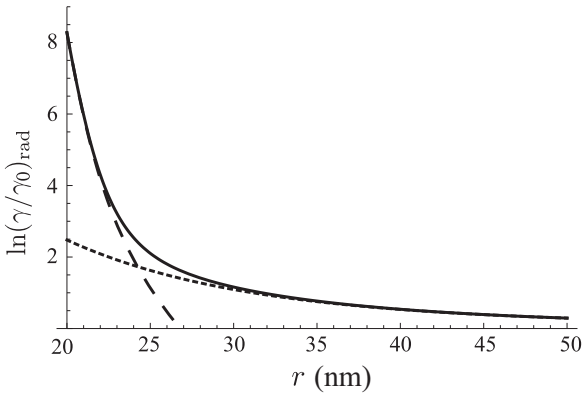

FIG. 2. Radial components of the normalized radiative (dotted line), nonradiative (dashed line), and total (solid line) decay rates for an atom coupled to the silver nanosphere of radius $a = 20$ nm at $\lambda = 632.8$ nm (see Fig. 1).

$$\Delta\omega_0 = \omega_0 - \omega_{\rm vac} = -\gamma_0\frac{3}{8}\frac{\varepsilon(\omega)-1}{(r|\mathbf{k}|)^4}\sum_{n=1}^{\infty}\frac{n(n+1)}{(\varepsilon+1)n+1}\left(\frac{a}{r}\right)^{2n} \times [2(n+2)a|\mathbf{k}|\cos^2\xi + n|\mathbf{k}|r\sin^2\xi], \tag{5}$$

where $\omega_{\rm vac} = 632.8$ nm is the atomic transition frequency in vacuum and ξ is the angle between the directions of the dipole moment and $\mathbf{r}$. The behavior of $\Delta\omega_0$ versus the spherical coordinates of the atom in the vicinity of a silver nanosphere is illustrated in Fig. 3(b). One can see that the normalized radiative frequency shift monotonically increases with decreasing distance between the atom and the nanosphere, showing a sharp drop in the vicinity of the angle $\theta = \pi/2$, which is vanishing at distances $r \geqslant 40$ nm. It is also worth noting that despite the radiative shift being rather small, it enters the analytical formula for the correlation functions for the photon-number statistics we calculate in the following sections as a dimensionless frequency shift, so its contribution to the nonclassical properties of light from resonance fluorescence will be essential.

Also important to mention is that, despite all formulas in this section for the decay rate and the radiative frequency shift of a two-level atom in close proximity to a metal nanosphere being derived in a very simple quasistatic, quasiclassical model, they fit well at a distance between the emitter and the surface of the nanoparticle not less than a few (2–5) nm, the results of a more detailed theoretical and numerical treatment within classical electrodynamics [35,36] and, recently, of fully quantum consideration [37–39]. The latter allows for a correct description of the strong coupling between the quantum emitter and a metal nanoparticle at very small distances to the nanoparticle's surface as well as accounting for the self-coupling of the quantum emitter through the metal nanoparticle [39].

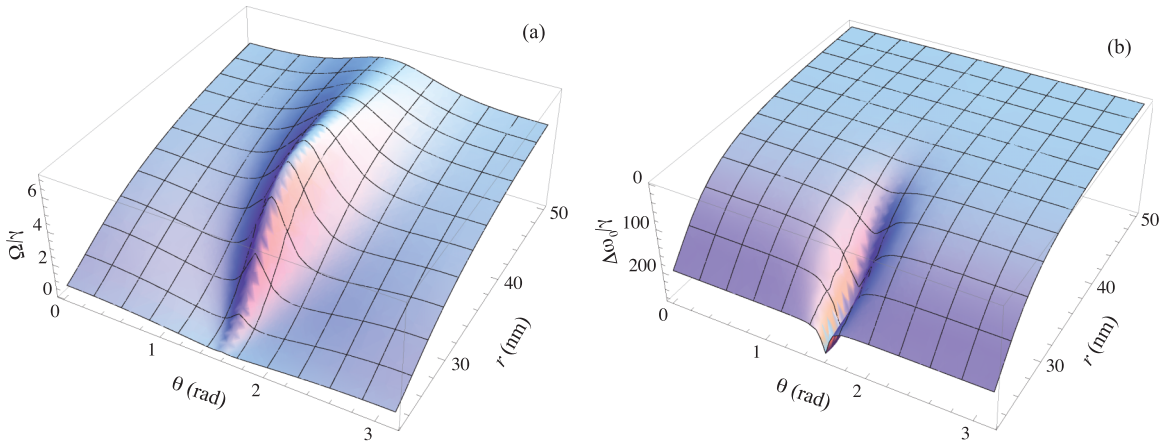

FIG. 3. (Color online) (a) Normalized Rabi frequency and (b) radiative frequency shift of the atomic transition versus the spherical coordinates of the atom in the vicinity of a silver nanosphere. All the parameters are the same as in Fig. 2.

III. RESONANCE FLUORESCENCE PHOTON-NUMBER STATISTICS OF A TWO-LEVEL ATOM NEAR A METAL NANOSPHERE

A. Theory

The photon-number statistics in resonance fluorescence from a two-level atom in free space driving by a monochromatic electromagnetic field was first considered by Mandel [2] and Lenstra [3]. Following these works, we will calculate the flux of the fluorescent photons registered in the far field in 4π, taking into account that the radiation properties of the atom are affected by a metal nanosphere and that the laser driving the system has a spectral width of $\Delta\omega_L$.

We start by calculating the intensity of the fluorescent light at point $\mathbf{r}$ at time t,

$$\langle \hat{I}'(\mathbf{r},t)\rangle = \left(\frac{1}{4\pi\varepsilon_0}\frac{\omega_0^2 d}{c^2 r}\right)^2\left(1-\frac{1}{2}\sin^2\theta\right) \times\left[\left\langle \hat{R}_3\left(t-\frac{r}{c}\right)\right\rangle+\frac{1}{2}\right], \tag{6}$$

where $\langle \hat{R}_3(t)\rangle = \frac{1}{2}[\hat{b}^\dagger(t)+\hat{b}(t)]$, $\hat{b}^\dagger(t)$ and $\hat{b}(t)$ are the raising and lowering operators, respectively, and the expression for $\hat{b}(t)$ for the arbitrary initial conditions can be found, for example, in [24]. Then the fluorescent photon flux density (in photons/m^2 s) operator [40]

$$\hat{I}''(\mathbf{r},t) = \frac{2\varepsilon_0\langle \hat{I}'(\mathbf{r},t)\rangle c}{\hbar\omega_0} \tag{7}$$

and its integration over a spherical angle gives the total photon flux in the corresponding spherical sector of radius r,

$$\begin{aligned}\hat{I}''_{\rm sec}(r,\theta_1,\theta_2,\phi_1,\phi_2,t) &= \int_{\phi_1}^{\phi_2} d\phi\int_{\theta_1}^{\theta_2}\hat{I}''(\mathbf{r},t)\sin\theta\, d\theta \\ &= \frac{2\varepsilon_0 c}{\hbar\omega_0}\left(\frac{1}{4\pi\varepsilon_0}\frac{\omega_0^2 d}{c^2 r}\right)^2\left[\left\langle \hat{R}_3\left(t-\frac{r}{c}\right)\right\rangle+\frac{1}{2}\right] \\ &\times\int_{\phi_1}^{\phi_2} d\phi\int_{\theta_1}^{\theta_2}\left(1-\frac{1}{2}\sin^2\theta\right)\sin\theta\, d\theta.\end{aligned} \tag{8}$$

The total fluorescence photon flux in 4π is then equal to

$$\hat{I}(\mathbf{r},t) = \frac{8\pi}{3}\hat{I}''(\mathbf{r},t). \tag{9}$$

The probability that n photons are emitted by an atom driven by an incident electromagnetic field within the time interval t to $t+T$ in 4π can be written as [2]

$$p(n,t,T) = \left\langle \mathcal{T} : \frac{1}{n!}\left[\int_t^{t+T} dt'\,\hat{I}(\mathbf{r},t)\right]^n \times\exp\left[-\int_t^{t+T} dt'\,\hat{I}(\mathbf{r},t)\right] : \right\rangle, \tag{10}$$

where $\mathcal{T}$ is the time-ordering symbol, : : stands for normal ordering, and $\langle\,\rangle$ denotes the expectation value for the total state of the atom plus nanoparticle plus driving field system. Correspondingly, the probability of photon emission in a spherical sector of radius r can be calculated using Eq. (10) by replacing $\hat{I}(\mathbf{r},t)$ with $\hat{I}''_{\rm sec}$. From now on, we will consider collecting the fluorescent photons in 4π. In this work we limit our consideration to a steady-state fluorescence, so $p(n,t,T) = p(n,T)$ in Eq. (10).

Following the derivation of formulas for the mean value of the fluorescent photons and the variance, we discuss now at what time scale the statistical distribution of fluorescent photons $p(n,T)$ converges in the distribution to the Gaussian one. In this paper we take into account that the atomic radiation properties are affected by the closely located metal nanosphere and that the incident laser has a spectral width $\Delta\omega_L$.

The statistical properties of the fluorescent radiation are described by a simple cumulant-generating function [3]

$$G(z,T) = \sum_{n=0}^{\infty} z^n\, p(n,T), \tag{11}$$

where the distribution $p(n,t)$ is given by Eq. (10). The rth factorial moment $\langle n^{(r)}\rangle$ can then be calculated from the generating function as

$$\langle n^{(r)}\rangle = \frac{d^r}{dz'}G(z,T)\bigg|_{z=1}, \tag{12}$$

resulting in analytical formulas for $\langle n^{(r)}\rangle$ given in the Appendix. The mean $\langle n\rangle=\langle n^{(1)}\rangle$ can be readily calculated from Eq. (12) and results in

$$\langle n\rangle = T\langle \hat{I}\rangle, \tag{13}$$

where $\langle \hat{I}\rangle$ is the total flux of the fluorescence photons at $t\to\infty$ equal to

$$\langle \hat{I}\rangle = \frac{(1/2)\beta\Omega^2(1+\Delta\omega_L/\beta)}{(1/2)\Omega^2(1+\Delta\omega_L/\beta)+(\beta+\Delta\omega_L)^2+\beta^2D^2}. \tag{14}$$

Here $\beta=\gamma/2$ [γ is the total decay rate of the two-level atom in close proximity to the metal nanosphere; see Eq. (2)] and $D=(\omega_L-\omega_0)/\beta$ is the dimensionless frequency detuning. Similarly, the variance is equal to

$$\begin{aligned}\sigma^2 &= \langle n^2\rangle - \langle n\rangle^2 \\ &= \langle n^{(2)}\rangle + \langle n\rangle - \langle n\rangle^2 \\ &= \sum_{i=1,i\neq j\neq k}^{3}\frac{\tilde{I}_i}{p_i}T - \sum_{i=1,i\neq j\neq k}^{3}\frac{\tilde{I}_i}{p_i^2}\left(e^{p_iT}-1\right)+\langle\hat{I}\rangle T,\end{aligned} \tag{15}$$

where

$$\begin{aligned}\tilde{I}_i = {}& \frac{\Omega^2(1+\Delta\omega_L/\beta)/2+(\beta+\Delta\omega_L)^2+\beta^2D^2}{\beta\Omega^2(1+\Delta\omega_L/\beta)/4} \\ & \times\frac{\beta(2\beta+p_i)[(\beta+\Delta\omega_L+p_i)^2+\beta^2D^2]}{2p_i(p_i-p_j)(p_i-p_k)},\end{aligned} \tag{16}$$

with $\langle\hat{I}\rangle$ being the steady-state fluorescence intensity defined by Eq. (14). For large T ($\geqslant 5/\beta$) we can neglect the exponential terms so that Eq. (15) simplifies to

$$\begin{aligned}\sigma^2 &= \sum_{i=1,i\neq j\neq k}^{3}\frac{\tilde{I}_i}{p_i}\left(T+\frac{1}{p_i}\right)+\langle\hat{I}\rangle T \\ &= \sum_{i=1,i\neq j\neq k}^{3}\frac{\tilde{I}_i}{p_i}\left(T+\frac{1}{p_i}\right)+\langle n\rangle.\end{aligned} \tag{17}$$

Analysis of Eqs. (13) and (17) for the mean $\langle n\rangle$ and the variance σ^2, respectively, clearly shows that both the mean and the variance are proportional to T for large values of T, which is in agreement with the results of Ref. [41].

As follows from Eq. (10), the function $p(n,T)$ can be rewritten as

$$p(m,T)=\frac{1}{m!}\sum_{r=0}^{\infty}\frac{(-1)^r}{r!}\langle n^{(m+r)}\rangle, \tag{18}$$

where $\langle n^{(0)}\rangle=1$. Analytical expressions for $\langle n^{(r)}\rangle$ and $p(n,T)$ for the arbitrary values of T and n are cumbersome and can hardly be used for a direct analysis. Instead, we will analyze the behavior of the distribution function in the limit of large counting times T. This can be suitably done by using the normalized variable

$$x_n=\frac{n-\langle n\rangle}{\sigma}\quad(n=0,1,2,\ldots) \tag{19}$$

and the corresponding cumulant generating function, which is related to $G(z,T)$ as

$$\begin{aligned}K(y,T) &= \ln\left[\sum_{n=0}^{\infty}e^{y(n-\langle n\rangle)/\sigma}\,p(n,T)\right] \\ &= -\langle n\rangle y/\sigma+\ln[G(e^{y/\sigma},T)].\end{aligned}$$

Expanding this function by powers of y, we have

$$K(y,T)=K_1y+K_2y^2+K_3y^3+K_4y^4+\cdots, \tag{20}$$

where $K_k\sim(T^{k-2})^{-1/2}$ [3].

This distribution function must converge with increasing counting time T, as we expect from the central limit theorem, to the Gaussian one

$$p(n,T)=\frac{1}{2\pi\sigma^2}\exp\left[\frac{-(n-\langle n\rangle)^2}{2\sigma^2}\right].$$

In the limit of $T\to\infty$, when there is a Gaussian-like distribution, all coefficients $K_i=0$ for $i\geqslant 3$, whereas at small counting times basically all $K_i\neq 0$ and the slowest decreasing cumulant in Eq. (20) is the third one.

Therefore, in our analysis of the time scale at which the distribution function converges to the Gaussian one, the most crucial role is played by the third cumulant K_3 for which our calculations give

$$\begin{aligned}K_3 &= \frac{1}{6}[s^{(1)}+6s^{(2)}+6s^{(3)}]T(y/\sigma)^3 \\ &= \frac{1}{6}\left[\frac{s^{(1)}+6s^{(2)}+6s^{(3)}}{6(s^{(1)}+2s^{(2)})^{3/2}}\right]T^{-1/2},\end{aligned} \tag{21}$$

where

$$s^{(1)}=\frac{\beta\Omega^2(\beta+\Delta\omega_L)}{2\beta(\beta+\Delta\omega_L)^2+2\beta^3D^2+\Omega^2(\beta+\Delta\omega_L)},$$

$$s^{(2)}=\frac{\beta\Omega^2s^{(1)}-[(\beta+\Delta\omega_L)^2+\beta^2D^2+4\beta(\beta+\Delta\omega_L)+\Omega^2](s^{(1)})^2}{2\beta(\beta+\Delta\omega_L)^2+2\beta^3D^2+\Omega^2(\beta+\Delta\omega_L)},$$

$$s^{(3)}=\frac{\beta\Omega^2(s^{(2)})^2}{2\beta(\beta+\Delta\omega_L)^2+2\beta^3D^2+\Omega^2(\beta+\Delta\omega_L)}-\frac{2[(\beta+\Delta\omega_L)^2+\beta^2D^2+4\beta(\beta+\Delta\omega_L)+\Omega^2]s^{(1)}s^{(2)}+(4\beta+2\Delta\omega_L)(s^{(1)})^3}{2\beta(\beta+\Delta\omega_L)^2+2\beta^3D^2+\Omega^2(\beta+\Delta\omega_L)},$$

where D is the frequency detuning from the atomic transition normalized to γ_0. A simple check of the formula (21) and expressions for $s^{(i)}$ without the metal nanoparticle and in the limit of $\Delta\omega_L\to 0$ shows that our equations coincide with those for a two-level atom in free space [3].

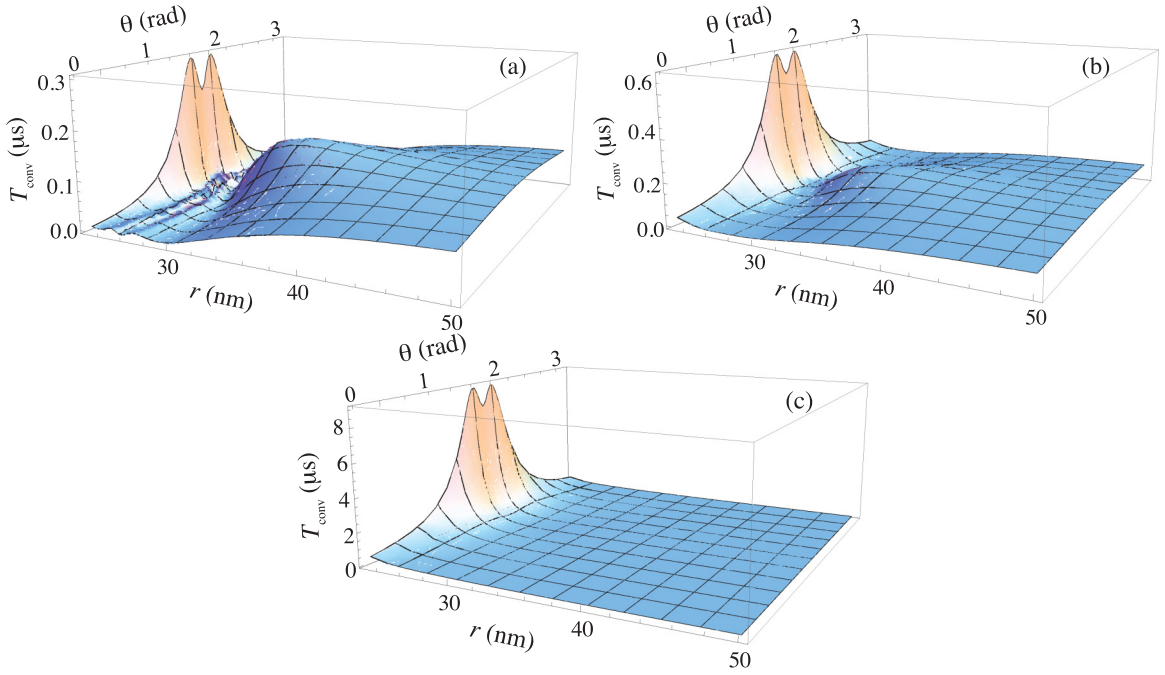

FIG. 4. (Color online) Dependence of the typical convergence time $T_{\rm conv}$ versus the atomic coordinates r (left) and θ (right) around the nanosphere and the normalized frequency detuning (a) $D = 0$, (b) $D = 1$, and (c) $D = 5$ at $\Delta\omega_L = 1$ MHz.

Let us assume that the skewness (third normalized central moment)

$$\left\langle \left(\frac{n - \langle n \rangle}{\sigma} \right)^3 \right\rangle = 6K_3$$

is a measure for the deviation of the actual distribution function $p(n,T)$ from its asymptotic Gaussian form. Then, as follows from Eq. (21), the typical time scale $T_{\rm conv}$ at which the distribution function converges to the Gaussian form is equal to

$$T_{\rm conv} = \frac{(s^{(1)} + 6s^{(2)} + 6s^{(3)})^2}{(s^{(1)} + 2s^{(2)})^3}. \tag{22}$$

B. Computer analysis

For further analysis of the analytical formulas for the convergence time, the distribution function, the mean value, and the variance, which we derived in the previous section, we will assume as in Sec. II that the plasmonic nanosphere is made of silver and has a radius of $r = 20$ nm and the incident laser field is linearly polarized along the z axis, has a bandwidth $\Delta\omega_L \lesssim \gamma$, and is detuned from the atomic transition at $D\gamma$. We will also limit our analysis to the distances between the atom and the nanoparticle's surface not less than 3 nm due to the restrictions imposed by the quasiclassical atom-nanoparticle coupling model we use (see Sec. II).

We start with analysis of Eq. (22) for the convergence time $T_{\rm conv}$, which depends on the parameters Ω, γ, D and $\Delta\omega_L$, i.e., on the location of the atom around the nanosphere, in a complicated way. Note, for reference, that for the atom in free space $T_{\rm conv} = 0.1$ μs.

Figure 4 illustrates the behavior of $T_{\rm conv}$ on the atomic coordinates r and θ around the nanosphere and the normalized detuning D for a finite bandwidth of the incident laser field. It shows that the convergence time essentially depends on the atomic coordinates around the nanosphere at the distances $r \leqslant 50$ nm for $D = 0$, 40 nm for $D = 1$, and 30 nm for $D = 5$, which essentially reflects the area where the near field of the metal nanosphere is essential. In the vicinity of $\theta = \pi/2$ the convergence time reaches its global maximum at $r = 23$ nm (we do not make our analysis at smaller distances, as our model for the decay rate is invalid there): $T_{\rm conv}^{\rm max} = 0.3$ μs for $D = 0$ to $T_{\rm conv}^{\rm max} = 9$ μs at $D = 5$, which is up to two orders of magnitude longer than for the atom in free space. Surely, at distances $r \gg a$, when the influence of the metal nanosphere is negligible, the convergence time approaches its value for the atom in free space, i.e., $I_{\rm conv} \to 0.1$ μs, which is clearly seen in Fig. 4.

In the areas around the nanosphere with $\Omega/\gamma \gg 1$ [see Fig. 3(a)], Eq. (22) simplifies to $T_{\rm conv} \approx 1/\beta = 2/\gamma$, i.e., the convergence time inversely depends on the modified decay rate of the atom coupled to the metal nanosphere. This behavior determines the local minimum in the three-dimensional graphs in Fig. 4 for $T_{\rm conv}$ at $23 \leqslant r \leqslant 40$ nm, which is more pronounced at $D = 0$ [Fig. 4(a)] and vanishes with increasing D to the value of 5 [Fig. 4(c)].

In the areas of $\Omega/\gamma \ll 1$ [see Fig. 3(a)], the resonance fluorescence spectrum features only one central peak [26,28] and studying the statistics of photons emitted in resonance fluorescence reveals information about the atom's location around the nanosphere and its coupling to the nanosphere. In this case, Eq. (22) simplifies to

$$T_{\rm conv} \approx \frac{1}{s^{(1)}} = \frac{2\beta(\beta + \Delta\omega_L)^2 + 2\beta^3 D^2 + \Omega^2(\beta + \Delta\omega_L)}{\beta\Omega^2(\beta + \Delta\omega_L)}, \tag{23}$$

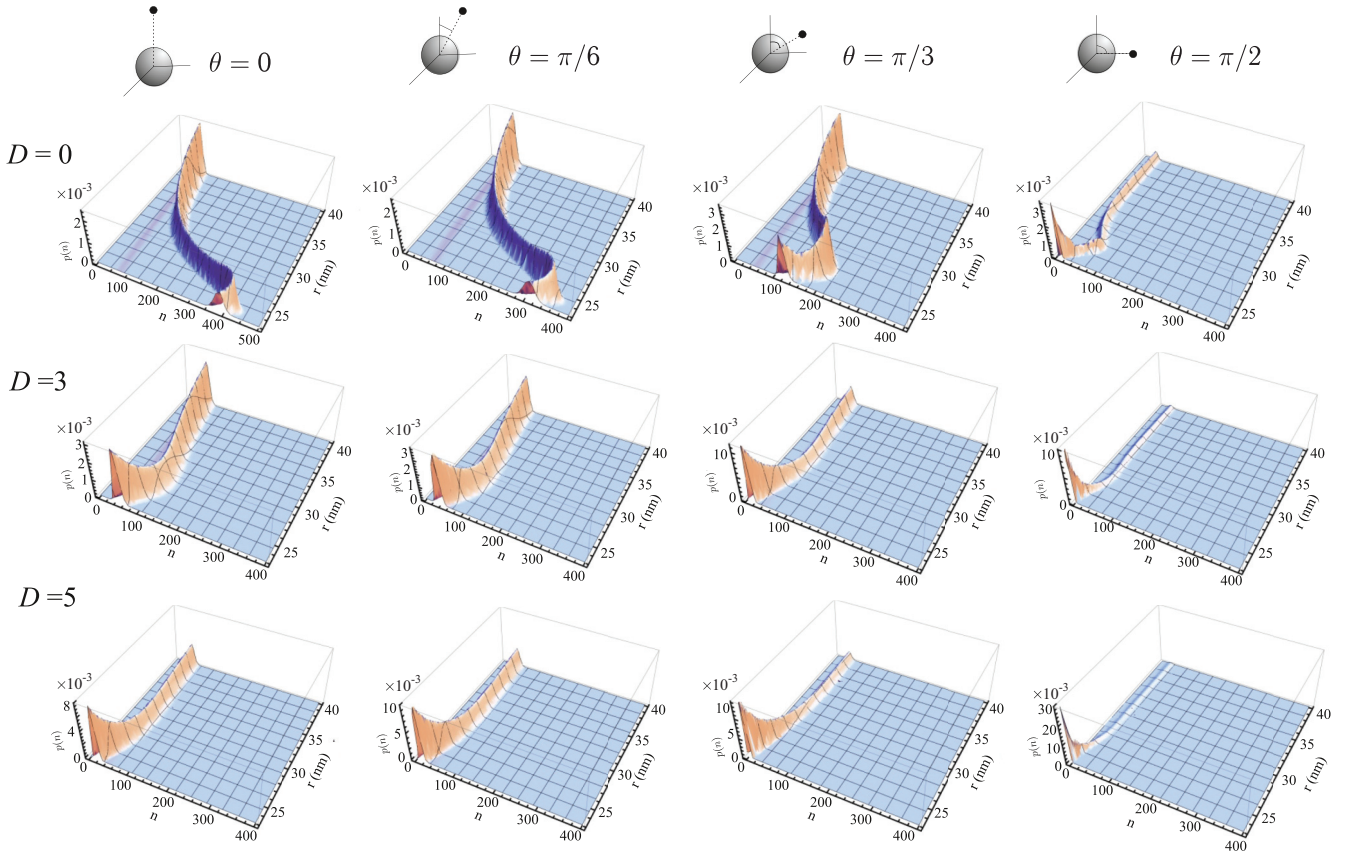

FIG. 5. (Color online) Probability $p(n,T)$ versus the radial coordinate r of the atom around the nanosphere at the azimuthal angles (from left to right) $\theta = 0, \pi/6, \pi/3$, and $\pi/2$ rad and for three values of the normalized frequency detuning (from top to bottom) $D = 0$, 3, and 5 for $T = 9\ \mu$s and $\Delta\omega_L = 1$ MHz.

which shows almost linear behavior versus the bandwidth $\Delta\omega_L$ and quadratic behavior versus the normalized frequency detuning D.

Analysis of the near field of the metal nanosphere shows also that there are two symmetrical areas in which $\Omega \sim \gamma$ and $T_{\rm conv} \approx 0$, which means that if the atom is located in such areas the photon-number distribution function will be Gaussian for any T. One of these areas has the polar coordinates (27 nm, 0.426 rad); the other one is located radially symmetrical.

The probability distribution function $p(n,T)$ for the steady-state resonance fluorescence versus the atom's location around the nanosphere is shown in Fig. 5. From this figure one can see that $p(n)$ drastically depends on the atom's location around the nanosphere, but preserves a characteristic twist in the

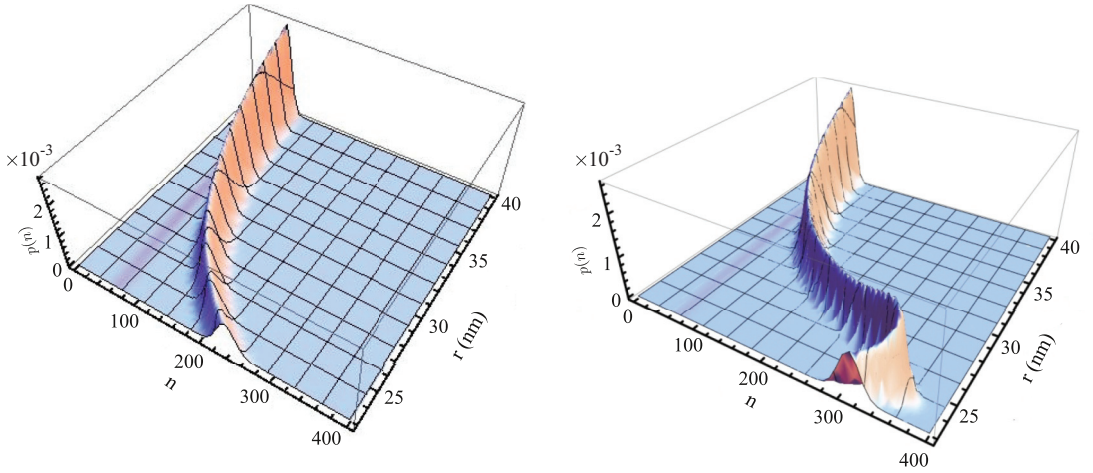

FIG. 6. (Color online) Probability $p(n,T)$ versus the radial coordinate r of the atom around the nanosphere for the case of an ideal sphere with $\varepsilon = -\infty$ (left) and for a silver sphere with $\varepsilon = -15.37 + i0.231$ (right) at the azimuthal angle $\theta = \pi/6$ rad for $T = 9\ \mu$s, $D = 0$, and $\Delta\omega_L = 1$ MHz.

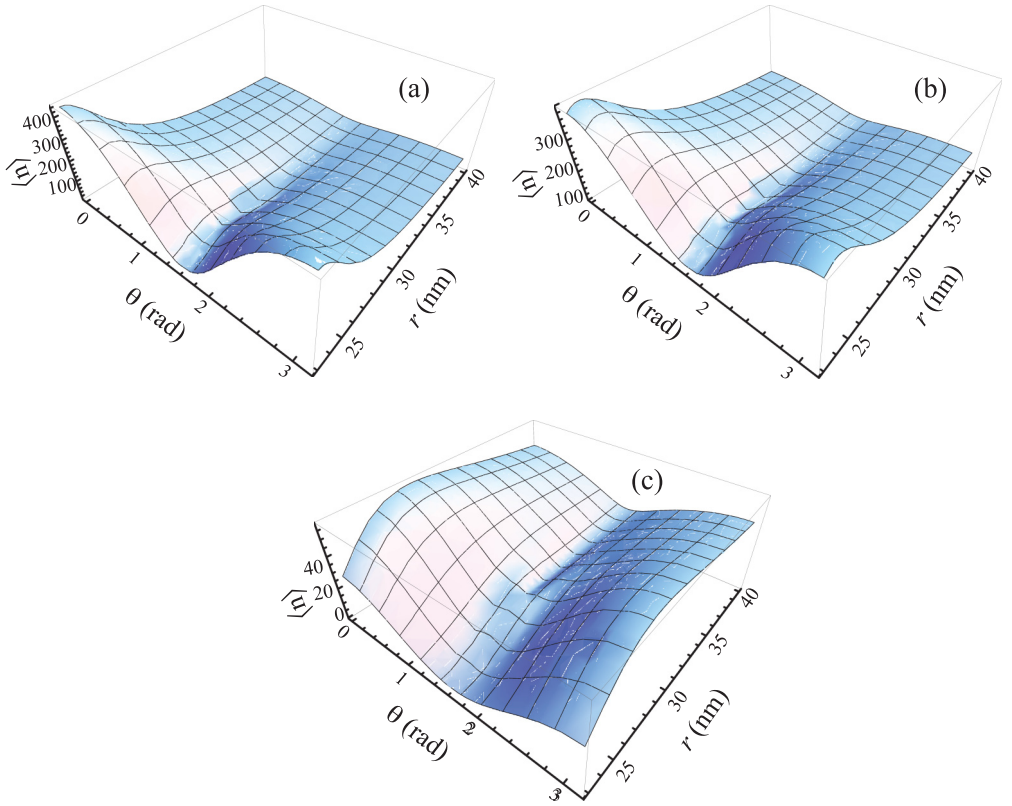

FIG. 7. (Color online) Mean value versus atomic coordinates r and θ around the nanosphere for the counting time $T = 9$ μs, $\Delta\omega_L = 1$ MHz, and (a) $D = 0$, (b) $D = 1$, and (c) $D = 5$.

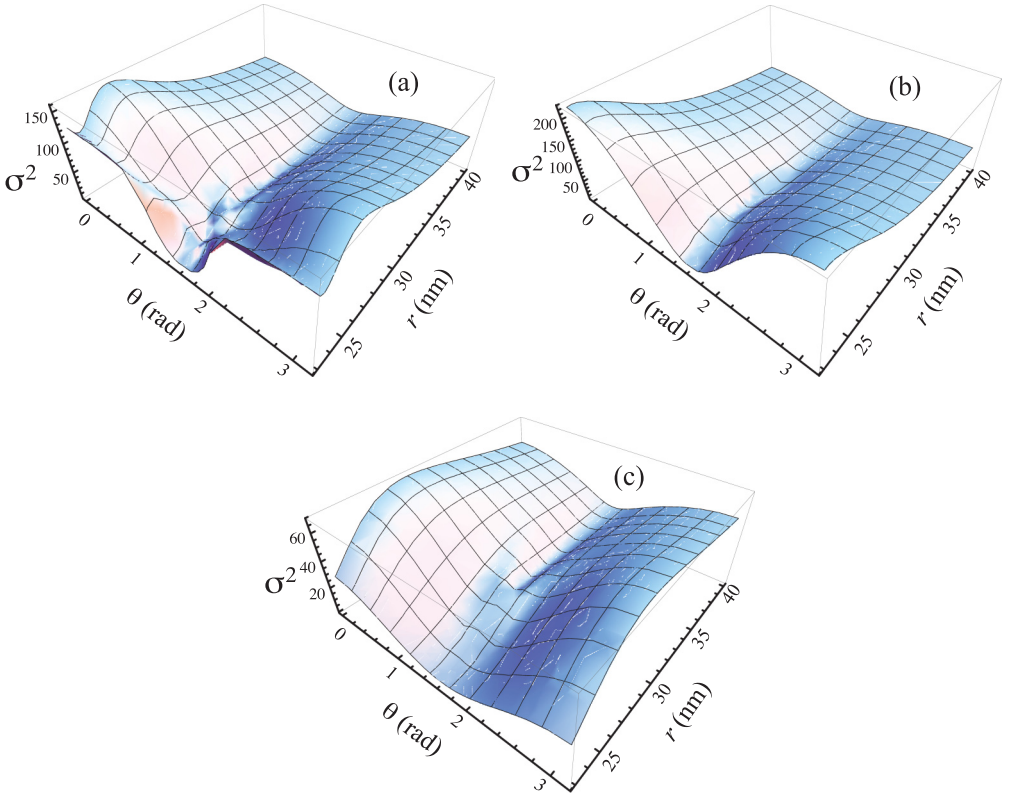

FIG. 8. (Color online) Variance versus atomic coordinates r and θ around the nanosphere for the counting time $T = 9$ μs, $\Delta\omega_L = 1$ MHz, and (a) $D = 0$, (b) $D = 1$, and (c) $D = 5$.

ridgelike dependence. In order to clarify the origin of this twist we calculated $p(n,T)$ for the fixed parameters $D = 0$ and $\theta = \pi/6$ (as for one of the plots in Fig. 5), but assuming that the nanosphere is made of either an ideal metal or silver. The results of these calculations are shown in Fig. 6. From this figure one can clearly see that the twist in the ridgelike dependence $p(n,T)$ is caused by the nonradiative part of the decay rate of the atom coupled to the metal nanosphere, which is essential in the range of $23 \leqslant r \leqslant 40$ nm and vanishes at larger distances (see Sec. II).

Further analysis of Fig. 5 reveals that with increasing normalized frequency detuning the drastic behavior of $p(n,T)$ at the atom's location around the nanosphere largely vanishes; it remains only as a visible dependence on r at $23 \leqslant r \leqslant 30$, where $p(n)$ reaches a minimum at smaller D and for $\theta = 0$ to $\pi/6$. This is again due to the interference between the radiative and nonradiative decay rates of the atom coupled to the metal nanosphere. Also important to note is that increasing the normalized frequency detuning D increases the number of counted photons from areas of the atom's location around the nanosphere with $23 \leqslant r \leqslant 25$–$28$ nm, depending on θ.

The mean value and the variance for $p(n,T)$ are illustrated in Figs. 7 and 8. One can clearly see that a small change in the atomic coordinates leads to significant changes of the mean value and the variance, so these values are very sensitive to the atom's location.

In the areas around the nanosphere where $\Omega/\gamma \gg 1$ [see Fig. 3(a)], the mean value, as follows from Eqs. (12) and (14), can be approximated as

$$\langle n \rangle = T\beta = T\gamma/2, \tag{24}$$

so at these conditions it is entirely determined by the observation time and the normalized atomic decay rate of the atom coupled to the metal nanosphere (see Fig. 2). Besides the fact that the total number of fluorescent photons counted during the convergence time is increased, in contrast to the case of a weak near-field limit, it is worth noting here that for these conditions the probability distribution function strongly depends on the normalized frequency detuning D of the incident laser field from the atomic resonance.

IV. CONCLUSION

In this paper we have studied theoretically how the photon-number statistics from resonance fluorescence of a two-level atom driven near resonance by a laser radiation of finite bandwidth is affected by a metal nanosphere in close proximity to the atom. Our analysis shows that all the interesting physics here takes place in a small area around the nanosphere where the near field and the atom-nanosphere coupling essentially affect the radiative properties of the atom. Our theoretical estimations and numerical modeling evaluate this area roughly as $r \leqslant 2a$, double the radius of the nanosphere. At larger distances, the influence of the nanoparticle vanishes and the atom tends to behave similarly to that in free space.

It was shown that the behavior of the convergence time in the area of $r \leqslant 2a$ is determined by the interplay of the radiative and nonradiative decay rates of the atom due to the coupling with the metal nanosphere and by the near-field intensity. Additional parameters are the normalized laser frequency detuning from the atomic resonance and the bandwidth of the incoming laser field.

Our atom-nanoparticle coupling model is not valid at distances between the atom and the particle's surface less than a few nanometers [42] (see Sec. II), so we limited our analysis to those distances for which at $\theta = \pi/2$ the convergence time features its global maximum of up to $T_{\text{conv}} = 9\ \mu$s (at $D = 5$), two orders of magnitude slower than for the atom in free space. In the area around the metal nanosphere with $\Omega/\gamma \gg 1$, the convergence time $T_{\text{conv}} = 2/\gamma$ and depends only on the decay rate. In the areas with $\Omega/\gamma \ll 1$ the convergence time depends linearly on $\Delta\omega_L$ and quadratically on D. There are also two areas symmetrical around the nanosphere (at $r = 27$ nm, $\theta = 0.426$ rad, and radially symmetrical) in which $\Omega \sim \gamma$ and $T_{\text{conv}} \approx 0$.

The distribution function $p(n,T)$ of the emission probability of n photons in a given time interval T in steady-state resonance fluorescence also drastically depends on the atom location around the nanosphere for $r \leqslant 2a$, featuring a characteristic twist in the ridgelike dependence, and for $r \gg a$ tends to that of the atom in free space, converging to a Gaussian distribution when T is much longer than the natural lifetime of the excited atom modified by the nanoparticle. The typical convergence time scale at large distances $r > 2a$ tends to the convergence time of the atom in free space $T_{\text{conv}} \to 0.1\ \mu$s. Similarly to the convergence time, this behavior is due to the interplay of the radiative and nonradiative decay rates of the atom and the near-field intensity. By increasing the normalized frequency detuning D from 0 to 5, this effect largely vanishes.

The mean value and the variance behave similarly, showing the peculiar dependence on the radial coordinates for $r \leqslant 2a$ and coinciding with those for the atom in free space for $r \gg a$. In the areas with $\Omega/\gamma \gg 1$, the mean value $\langle n \rangle = T\gamma/2$ and is entirely determined by the observation time and the atomic decay rate. It is important also to mention that a small change in the atomic coordinates leads to significant changes of the mean value and the variance, so these values are very sensitive to the atom's location.

Finally, we intentionally used in our computer simulations the incident laser field wavelength $\lambda = 632.8$ nm, which is far from the plasmon resonance in the silver nanosphere of 20 nm radius that is achieved at $\approx$360 nm, as this is a regular experimental situation, when driving the atom-nanoparticle laser field system cannot be resonant with both the atomic transition and the plasmon resonance of the plasmonic nanoparticle. However, analysis of the atom–plasmonic-nanoparticle system, when the plasmon resonance in the nanoparticle is excited with the help of a laser field and the atom is driven by another near resonance to the atomic transition laser field, is also within the realm of experimental techniques and deserves separate consideration.

In conclusion, we demonstrated that quantum-optical properties of photons from an atom in a confined geometry driven by a near-resonance laser provide valuable and sensitive information about the coupling of an atom with the

nanoenvironment and should stimulate future experiments in this field.

ACKNOWLEDGMENTS

The authors acknowledge funding from the Russian Foundation for Basic Research under Grant No. 13-02-00446.

APPENDIX: CALCULATION OF THE CUMULANT-GENERATING FUNCTION $G(z,T)$

Statistical properties of the fluorescent radiation are described by a simple cumulant-generating function [3]

$$G(z,T)=\sum_{n=0}^{\infty} z^n p(n,T),$$

where the distribution $p(n,t)$ is given by Eq. (10). Keeping in mind that the nth-order correlation function can be interpreted as the joint probability of the photon emission at n different successive moments $t_1<t_2<\cdots<t_n$ and assuming that the atom returns to the ground state after each spontaneous emission and has no memory of the earlier event, the generation function (11) further simplifies to

$$G(z,T)=1+2\beta(z-1)\int_0^T dt f(t)+\sum_{n=2}^{\infty}(2\beta)^n(z-1)^n \times\int_0^T dt_n\int_0^{t_n} dt_{n-1}\cdots\int_0^{t_2} dt_1 f_0(t_n-t_{n-1}) \times f_0(t_{n-1}-t_{n-2})\cdots f_0(t_2-t_1)f(t_1), \quad \text{(A1)}$$

where $f(t)=\langle\hat{I}(t)\rangle/2\beta$ and $f_0(t)=\langle\hat{I}(t)\rangle_{0;G}/2\beta$ are the dimensionless functions ($t\geqslant 0$) and the notation $\langle\,\rangle_{t;G}$ stands for the expectation value for the atom in the ground state at t.

Multiple integration in Eq. (A1) can be handled with the help of the Laplace transformation [43], which after applying it to both sides of Eq. (A1) with respect to T gives

$$\tilde{G}(z,s)=\frac{C(s)+\beta(z-1)B(s)}{sC(s)-\beta\Omega^2(z-1)(s+\beta+\Delta\omega_L)}, \quad \text{(A2)}$$

with

$$C(s)=s^3+s^2(4\beta+2\Delta\omega_L) +s[(\beta+\Delta\omega_L)^2+\beta^2D^2+4\beta(\beta+\Delta\omega_L)+\Omega^2] +[2\beta(\beta+\Delta\omega_L)^2+2\beta^3D+\Omega^2(\beta+\Delta\omega_L)],$$

$$B(s)=2\beta[\tilde{f}(s)-\tilde{f}_0(s)]C(s),$$

where $\tilde{f}(s)$ and $\tilde{f}_0(s)$ are the Laplace transforms for $f(t)$ and $f_0(t)$ in Eq. (A1), respectively. The generation function $G(z,T)$ can be obtained then by applying the inverse Laplace transform to Eq. (A2) [43].

[1] L. Davidovich, Rev. Mod. Phys. **68**, 127 (1996).
[2] L. Mandel, Opt. Lett. **4**, 205 (1979).
[3] D. Lenstra, Phys. Rev. A **26**, 3369 (1982).
[4] H. J. Kimble, M. Dagenais, and L. Mandel, Phys. Rev. Lett. **39**, 691 (1977).
[5] R. Short and L. Mandel, Phys. Rev. Lett. **51**, 384 (1983).
[6] F. Diedrich and H. Walther, Phys. Rev. Lett. **58**, 203 (1987).
[7] S. V. Gaponenko, *Introduction to Nanophotonics* (Cambridge University Press, New York, 2010).
[8] Th. Basché, W. E. Moerner, M. Orrit, and H. Talon, Phys. Rev. Lett. **69**, 1516 (1992).
[9] L. Fleury, J.-M. Segura, G. Zumofen, B. Hecht, and U. P. Wild, Phys. Rev. Lett. **84**, 1148 (2000).
[10] S. Buckley, K. Rivoire, and J. Vučcckovič, Rep. Prog. Phys. **75**, 126503 (2012).
[11] P. Michler, A. Imamoğlu, M. D. Mason, P. J. Carson, G. F. Strouse, and S. K. Buratto, Nature (London) **406**, 968 (2000).
[12] O. Astafiev, A. M. Zagoskin, A. A. Abdumalikov, Yu. A. Pashkin, T. Yamamoto, K. Inomata, Y. Nakamura, and J. S. Tsai, Science **327**, 840 (2010).
[13] A. Ulhaq, S. Weiler, S. M. Ulrich, R. Roßbach, M. Jetter, and P. Michler, Nat. Photon. **6**, 238 (2012).
[14] A. Ulhaq, S. Weiler, C. Roy, S. M. Ulrich, S. Hughes, and P. Michler, Opt. Express **21**, 4382 (2013).
[15] V. N. Molchalin, O. Shenderova, D. Ho, and Y. Godotsi, Nat. Nanotechnol. **7**, 11 (2012).
[16] N. Mizuochi, T. Makino, H. Kato, D. Takeuchi, M. Ogura, H. Okushi, M. Nothaft, P. Neumann, A. Gali, F. Jelezko, J. Wrachtrup, and S. Yamasaki, Nat. Photon. **6**, 299 (2012).
[17] A. Sommerfeld, Ann. Phys. (Leipzig) **333**(4), 665 (1909).
[18] E. M. Purcell, H. C. Torrey, and R. V. Pound, Phys. Rev. **69**, 37 (1946).
[19] V. V. Klimov, *Nanoplasmonics: Fundamentals and applications* (Pan Stanford, Singapore, 2012).
[20] S. A. Maier, *Plasmonics: Fundamentals and Applications* (Springer, New York, 2007).
[21] P. Zijlstra and M. Orrit, Rep. Prog. Phys. **74**, 106401 (2011).
[22] H. A. Altwater, Sci. Am. **296** (4), 56 (2007).
[23] B. Hecht and L. Novotny, *Principles of Nano-Optics* (Cambridge University Press, Cambridge, 2006).
[24] H. J. Kimble and L. Mandel, Phys. Rev. A **13**, 2123 (1976).
[25] Y. Gu, L. Huang, O. J. F. Martin, and Q. Gong, Phys. Rev. B **81**, 193103 (2010).
[26] Y. V. Vladimirova, V. V. Klimov, V. M. Pastukhov, and V. N. Zadkov, Phys. Rev. A **85**, 053408 (2012).
[27] A. Ridolfo, O. Di Stefano, N. Fina, R. Saija, and S. Savasta, Phys. Rev. Lett. **105**, 263601 (2010).
[28] R.-C. Ge, C. Van Vlack, P. Yao, J. F. Young, and S. Hughes, Phys. Rev. B **87**, 205425 (2013).
[29] J. I. Cirac, R. Blatt, A. S. Parkins, and P. Zoller, Phys. Rev. A **48**, 2169 (1993).
[30] C. Cohen-Tannoudji and S. Reynaud, J. Phys. B **10**, 345 (1977).
[31] Yu. V. Vladimirova, B. A. Grishanin, V. N. Zadkov, N. N. Kolachevskii, A. V. Akimov, N. A. Kisilev, and S. I. Kanorskii, J. Exp. Theor. Phys. **96**, 629 (2003).

[32] M. S. Agronovich, B. Z. Katsenelbaum, A. N. Sizov, and N. N. Voitovich, *Generalized Method of Eigenoscillations in Diffrraction Theory* (Wiley-VCH, Berlin, 1999).
[33] E. D. Chubchev, Yu. V. Vladimirova, and V. N. Zadkov, Opt. Express **22**, 20432 (2014).
[34] V. V. Klimov, M. Ducloy, and V. S. Letokhov, J. Mod. Opt. **43**, 2251 (1996).
[35] F. Kaminski, V. Sandoghdar, and M. Agio, J. Computat. Theor. Nanosci. **4**, 635 (2007).
[36] M. Sukharev, N. Freifeld, and A. Nitzan, J. Phys. Chem. C **118**, 10545 (2014).
[37] V. N. Pustovit and T. V. Shahbazyan, J. Chem. Phys. **136**, 204701 (2012).
[38] A. Delga, J. Feist, J. Bravo-Abad, and F. J. Garcia-Vidal, Phys. Rev. Lett. **112**, 253601 (2014).
[39] F. Tork Ladani, S. Campione, C. Guclu, and F. Capolino, Phys. Rev. B **90**, 125127 (2014).
[40] L. Mandel and E. Wolf, *Optical Coherence and Quantum Optics* (Cambridge University Press, Cambridge, 1995).
[41] H. F. Arnoldus and G. Nienhuis, Opt. Commun. **54**, 95 (1985).
[42] In an experiment, such an arrangement for which an atom cannot be located closer than a few nanometers from the metal nanoparticle's surface can easily be achieved by using the metal nanoparticles covered by a spacer of a few nanometers made of a dielectric material.
[43] B. Davies *Integral Transforms and Their Applications* (Springer, New York, 2002).